NUCL SCI TECH (2021) 32:70
https://doi.org/10.1007/s41365-021-00905-y

# Radiation-induced cross-linking: a novel avenue to permanent 3D modification of polymeric membranes

**Yu Gu**[1,2,3] · **Bo-Wu Zhang**[2] · **Zhen Guo**[1,3] · **Ji-Hao Li**[1] · **Ming Yu**[2] ·
**Lin-Fan Li**[1] · **Jing-Ye Li**[1,2]

Received: 15 March 2021 / Revised: 16 April 2021 / Accepted: 13 May 2021 / Published online: 7 July 2021

**Abstract** Membrane fouling is always the biggest problem in the practice of membrane separation technologies, which strongly impacts their applicability, separation efficiency, cost effectiveness, and service lifespan. Herein, a simple but effective 3D modification approach was designed for permanently functionalizing polymeric membranes by directly cross-linking polyvinyl alcohol (PVA) under gamma-ray irradiation at room temperature without any additives. After the modification, a PVA layer was constructed on the membrane surface and the pore inner surface of polyvinylidene fluoride (PVDF) membranes. This endowed them with good hydrophilicity, low adsorption of protein model foulants, and easy recoverability properties. In addition, the pore size and distribution were customized by controlling the PVA concentration, which enhanced the rejection ability of the resultant membranes and converted them from microfiltration to ultrafiltration. The cross-linked PVA layer was equipped with the resultant membranes with good resistance to chemical cleaning by acidic, alkaline, and oxidative reagents, which could greatly prolong the membrane service lifetime. Furthermore, this approach was demonstrated as a universal method to modify PVDF membranes with other hydrophilic macromolecular modifiers, including polyethylene glycol, sodium alginate, and polyvinyl pyrrolidone. This modification of the membranes effectively endowed them with good hydrophilicity and antifouling properties, as expected.

**Keywords** Ultrafiltration membrane · Antifouling · 3D modification · Gamma-ray · Cross-linking

## 1 Introduction

Functional modification is a topic of great concern in the research and development of various polymer membrane materials. Many membrane fouling problems, greatly affecting the applicability of membrane processes and the separation efficiency, cost effectiveness, and service lifespan of membranes [1–3], can be solved by functional modification. Generally, to mitigate membrane fouling, a modification is carried out to minimize the interactions of foulants with the membrane surface by regulating the surface chemical composition [1, 2] and the tailor surface morphological architecture. This is performed by smoothening the membrane roughness [4, 5] and by optimizing pore size and distribution [6, 7]. Finally, antifouling or nonfouling membrane materials are obtained. To date, many approaches have been used to design antifouling

---

This work was supported by the National Natural Science Foundation of China (Nos. 11875313, 12075153, and 11575277).

**Supplementary Information** The online version contains supplementary material available at https://doi.org/10.1007/s41365-021-00905-y.

✉ Bo-Wu Zhang
zhangbowu@shnu.edu.cn

✉ Jing-Ye Li
jyli@shnu.edu.cn

[1] Shanghai Institute of Applied Physics, Chinese Academy of Sciences, Shanghai 201800, China

[2] MOE Key Laboratory of Resource Chemistry and Shanghai Key Laboratory of Rare Earth Functional Materials, College of Chemistry and Materials Science, Shanghai Normal University, Shanghai 200234, China

[3] University of Chinese Academy of Sciences, Beijing 100049, China

membrane materials, including blending [8, 9], surface coating [10–12], and chemical grafting (to or from) [13–15]. However, most of them are only able to modify the physicochemical properties of the membrane surface (i.e., 2D modification), but it is difficult to decorate the inner surface of the pores [16].

In practice, besides external fouling on the membrane surface, fouling in membrane pores (i.e., internal fouling) is non-negligible and even crucial to membrane performance. This is because some small-size organic foulants tend to infiltrate into membrane pores, which are subsequently adsorbed and aggregated on the inner surface of the pores, resulting in rock-ribbed pore blocking or downsizing [17]. Internal membrane fouling is often difficult to remove by a washing process, leading to an unrecoverable decline in permeation and a sharp drop in the service lifespan. Therefore, a 3D modification method that can simultaneously decorate the membrane surface and the pore inner surface is required to engineer antifouling membrane materials. Surface segregation is a common and simple method to modify membrane materials three-dimensionally [18]. However, membranes prepared by this method cannot provide long-lasting antifouling properties because of the lack of strong interactions (such as covalent bonds) between the membrane and modifiers, which leads to modifier leakage during filtration operations [18]. Many amphoteric polymeric modifiers with block, comb, or branched structures were synthesized through complicated processes to maintain modifier stability in the membrane matrices [19]. However, they still cannot guarantee permanent antifouling properties. It is known that covalent bonding between modifiers and the membrane can improve the modifier stability in/on the matrix and provide composite excellent durability in use [20]. Therefore, a new 3D modification method is imperative to covalently anchor modifiers onto membrane matrices in order to prevent the modifier leakage.

Owing to their high energy, gamma-rays can create reactive carbon-centered radicals on polymer skeletons by direct or indirect attack on target chemical bonds under mild conditions [21]. These radicals easily initiate redox reactions, grafting polymers onto substrates or cross-linking between polymeric chains [22, 23]. This phenomenon has led to the widespread application of radiation technology for tailoring the performance of materials, either in bulk or on surfaces [24, 25]. To date, high-energy radiation-induced grafting methods have been widely investigated for membrane preparation and modification [26]. In addition, membranes manufactured by these methods have shown great potential in many industrial applications, such as energy storage and conversion [27] and substance separation and purification [24]. Considering that radiation-induced grafting reactions mainly follow radical mechanisms [28], modifiers for grafting are highly restricted by the availability of vinyl-containing compounds, which hinders the application of radiation-induced grafting methods. In contrast, radiation-induced cross-linking is not limited to vinyl cross-linkers. Some polymers with higher *G*-values for cross-linking ($G_X$) than those for scission ($G_S$) can be directly cross-linked under irradiation but without any cross-linking promoters [29]. For instance, sodium-exchanged Nafion® membranes were directly cross-linked under airtight conditions by temperature-controlled gamma-ray irradiation to form a network structure [30]. However, for separation applications, radiation-induced direct cross-linking to modify membrane materials has been neglected thus far.

Inspired by this, herein, we designed a simple and effective approach to modify polyvinylidene fluoride (PVDF) membranes three-dimensionally by covalently anchoring polyvinyl alcohol (PVA) with the assistance of gamma-ray irradiation. In this way, a hydrophilic gelation layer was formed on the membrane surface and the inner surface. Compared with the coating or blending methods, this design based on radiation-induced cross-linking between polymeric modifiers and membranes avoids the compatibility problem of polymeric mixtures [31, 32], especially, the poor compatibility between PVDF and PVA due to differences in solubility parameters ($\delta$) [33]. Additionally, the covalent bonding between PVA and the PVDF membrane enhances the functional durability of the modified membranes. In this work, micromorphological examinations were carried out to investigate the effect of PVA attachment on the surface roughness, pore size, and internal structure of the membranes. Bovine serum albumin (BSA) and lysozyme were used as model bio-foulants to evaluate the antifouling performance of the modified membranes by static adsorption, dynamic cross-flow fouling experiments, and fouling-backwashing cycle filtration tests. Subsequently, the chemical stabilities of the modified membranes were tested under highly acidic, alkaline, and oxidative conditions to assess their tolerance to harsh chemical cleaning. Moreover, polyethylene glycol (PEG), sodium alginate (SA), and polyvinyl pyrrolidone (PVP) were used as modifiers to directly modify PVDF membranes under gamma-ray irradiation in order to assess the universality of the designed method.

## 2 Experimental

### 2.1 Radiation-induced 3D modification of PVDF membranes

PVDF membranes were first cleaned by 1 h ethanol immersion and subsequently washed thrice with water.

After soaking in a PVA aqueous solution for 1 h at room temperature, the PVA-infused membranes were taken out from the PVA solution and vacuum-encapsulated in polyethylene bags using a heat sealer. The sealed bags were then treated by gamma-ray irradiation from a Cobalt-60 source at room temperature (~ 25 °C) and 200 kGy of absorbed dose for 17 h. Finally, the irradiated membranes were scraped and washed in hot water at 80 °C to remove the hydrogel on the membrane surface and then soaked in 50 °C water for 48 h (water was changed every 6 h). The obtained PVDF membranes with a PVA gelation layer (denoted as G-PVDF membranes) were stored in water for testing. To measure the loading of PVA on the obtained G-PVDF membranes, the degree of gelation (DG) was defined as follows:

$$G(\%) = \frac{W_G - W_O}{W_O} \times 100, \tag{1}$$

where $G(\%)$ represents the DG of the obtained membranes and $W_O$ (g) and $W_G$ (g) are the dry weights of the PVDF membranes before and after surface gelation under gamma-ray irradiation, respectively. G-PVDF membranes with different DGs were prepared using PVA aqueous solutions with different concentrations (1, 2.5, 5, and 7.5 wt%) under the same radiation conditions. Additionally, PEG, SA, and PVP aqueous solutions were separately prepared with a concentration of 2.5 wt% and were used to modify PVDF membranes by the same process as that of the PVA solution.

## 2.2 Porosity testing of membranes

First, the membrane was completely immersed in pure water for 12 h, and the wet membrane weight ($W_w$) was recorded after removing excess surface water. The membrane was then placed in a vacuum oven at 60 °C for 48 h to obtain the dry weight ($W_d$). The membrane porosity was obtained using Eq. (2) [34]:

$$\varepsilon(\%) = \frac{W_w - W_d}{Sh\rho} \times 100, \tag{2}$$

where $S$ and $h$ denote the area (cm$^2$) and thickness (cm) of the wet membranes, respectively, and $\rho$ is the density of water (g·cm$^{-3}$).

## 2.3 Testing of the molecular weight cut-off, mean effective pore size, and pore size distribution

By ignoring the interactions between solutes and membrane pores, the molecular weight cut-off (MWCO), mean effective pore size ($\mu_p$), and pore size ($d_p$) distribution of the membranes were evaluated via solute separation experiments using a series of aqueous feed solutions containing 100 ppm of neutral solutes. Here, poly(ethylene glycol) (PEG) with average molecular weights of 11,000 g·mol$^{-1}$ (11 kDa) and 20,000 g·mol$^{-1}$ (20 kDa) and poly(ethylene oxide) (PEO) with average molecular weights of 100,000 g·mol$^{-1}$ (100 kDa), 300,000 g·mol$^{-1}$ (300 kDa), and 600,000 g·mol$^{-1}$ (600 kDa) were used. The solute concentrations in the feed and permeate were determined using a chemical oxygen demand tester (DRB 200, Hach Co., Loveland, CO, USA). The relationship between the Stokes diameter ($d_s$, nm) and the molecular weight ($M$, g·mol$^{-1}$) follows the equations [35]:

for PEG,

$$d_s = 33.46 \times 10^{-12} \times M^{0.557}, \tag{3}$$

and for PEO,

$$d_s = 20.88 \times 10^{-12} \times M^{0.587}. \tag{4}$$

There is a linear relationship between the normal-logarithm representation of the solute rejection ($R$) and solute $d_s$. Therefore, the $\mu_p$ was defined as the $d_s$ at $R$ = 50%, and the geometric standard deviation ($\sigma_p$) was determined as the ratio of the $d_s$ at $R$ = 84.13% over that at $R$ = 50%. The MWCO was the solute molecular weight that was 90% rejected by the membrane ($R$ = 90%) [35]. On the basis of the $\mu_p$ and $\sigma_p$, the pore size distribution is expressed as the probability density function [35]:

$$\frac{dR(d_p)}{dd_p} = \frac{1}{d_p \ln \sigma_p \sqrt{2\pi}} \exp\left[-\frac{(\ln d_p - \ln \mu_p)^2}{2(\ln \sigma_p)^2}\right]. \tag{5}$$

## 2.4 Filtration experiments

The permeation properties of all prepared membranes were tested using a cross-flow unit in a Convergence Inspectors microfiltration (MF) and ultrafiltration (UF) pilot system (Poseidon, Convergence Inspector Co., USA). The tests were performed at room temperature under a transmembrane pressure of 1 bar ($p$). The water permeance was tested for 60 min and calculated using Eq. (6):

$$F(\mathrm{L \cdot m^{-2} \cdot h^{-1} \cdot bar^{-1}}) = \frac{\Delta V}{Ap\Delta t}, \tag{6}$$

where $\Delta V$ is the change in permeation volume (L) at the testing time $\Delta t$ (h) and $A$ is the effective membrane area (12.56 cm$^2$). At least, three samples were measured and averaged for each test.

## 2.5 Fouling resistance evaluation of membranes

To evaluate the membrane fouling resistance, a static protein fouling test was performed through BSA static adsorption in an aqueous solution. The membranes with a diameter of 50 mm were immersed in 60 mL of a BSA phosphate buffer solution (0.5 $g\cdot L^{-1}$, pH ~ 7.4) and incubated under moderate oscillation at room temperature. After 12 h incubation, the membranes were removed, and the concentration of residual BSA was determined by measuring the absorbance at 280 nm using a UV–Vis absorption spectrometer (UV-2600, Shimadzu Corp., Kyoto, Japan). Triplicate tests were performed for each sample and averaged. The BSA absorption on the membranes was calculated according to Eq. (7):

$$Q(\mu g \cdot cm^{-2}) = \frac{V(c_o - c_d)}{2S} \times 1000, \tag{7}$$

where $Q$ is the BSA adsorption of membranes ($\mu g\cdot cm^{-2}$), $C_0$ and $C_d$ are the BSA concentrations ($g\cdot L^{-1}$) in the buffer solution before and after adsorption, respectively, $V$ (L) is the volume of the BSA buffer solution, and $S$ ($cm^2$) is the membrane area.

For dynamic filtration fouling tests, loop filtration experiments were performed on the above-mentioned MF and UF pilot system. First, pure water permeance ($J_{w1}$) was tested through 60 min of water cross-flow filtration under a transmembrane pressure of 1 bar. Second, a BSA or lysozyme (1 $g\cdot L^{-1}$, pH ~ 7.4) buffered solution was used as the feed solution and filtered through the membrane above for another 60 min to measure the flux ($J_P$) under 1 bar. Subsequently, the membrane was unloaded from the device and backwashed with water for 15 min to recycle the membrane. Next, the water permeance of the recycled membrane ($J_{w2}$) was tested as in the first step. This filtration-in-series model was used to assess the membrane fouling resistance calculated as follows [36]:

$$FR(\%) = \frac{J_{w2}}{J_{w1}} \times 100, \tag{8}$$

$$R_r(\%) = \frac{J_{w2} - J_P}{J_{w1}} \times 100, \tag{9}$$

$$R_{ir}(\%) = \frac{J_{w1} - J_{w2}}{J_{w1}} \times 100, \tag{10}$$

$$R_t(\%) = \frac{J_{w1} - J_P}{J_{w1}} \times 100, \tag{11}$$

where $R_t$ represents the total fouling ratio, $R_{ir}$ is the irreversible fouling ratio, and $R_r$ is the reversible fouling ratio.

### 2.6 Chemical resistance test of membranes

Generally, chemical cleaning is the main harsh chemical condition that membrane materials must endure during application. Herein, NaClO (2 $g\cdot L^{-1}$), HCl (1 $mol\cdot L^{-1}$), and NaOH (1 $mol\cdot L^{-1}$) aqueous solutions were used as the harsh reagents to test the resistance of the membranes to chemical corrosion. Pristine PVDF, i-PVDF, and G-PVDF-2 membranes were immersed in the solutions above for 24 h. The color changes of the membranes were recorded and measured by *Lab* values, which were acquired using a colorimeter (NR10QC, Shenzhen 3nh Technology Co., Ltd., Shenzhen, China). After soaking in the harsh solutions, the membranes were fully washed and stored in pure water.

## 3 Results and discussion

### 3.1 Characterization of membranes modified by PVA in situ gelation

As shown in Fig. 1a, the PVDF membranes were first infused with a PVA solution, then gamma-ray irradiated at 200 kGy of the total absorbed dose for 17 h, and purified by hot water until there was no additional weight loss (Fig. S1a). Finally, PVDF membranes with a PVA gelation layer (i.e., G-PVDF membranes) were obtained. G-PVDF membranes with DGs were prepared by soaking the PVDF membranes in PVA solutions with different concentrations (1, 2.5, 5, and 7.5 wt%). The DGs of the corresponding membranes were 1.3, 2.1, 6.3, and 8.4%, respectively. For brevity, the membranes were named G-PVDF-1, G-PVDF-2, G-PVDF-6, and G-PVDF-8 membranes, respectively. The DGs of these membranes were found to be positively correlated with the PVA concentration (Figs. S1b and S2), which agreed well with the *G*-value trend of PVA intermolecular cross-linking by gamma-ray irradiation [37]. Chemical composition analysis by Fourier transform-infrared (FT-IR) spectroscopy and X-ray photoelectron spectroscopy (XPS) confirmed the successful anchoring of PVA onto the PVDF membrane surfaces (Figs. S3 and S4) [38, 39].

Membrane micromorphology was observed by scanning electron microscopy (SEM) and atomic force microscopy (AFM). The membrane surfaces were found to be successfully covered by a PVA gelation layer, and the rich pothole-like morphology of the pristine PVDF membrane surfaces was visibly smoother after PVA modification (Figs. 1b–d). As a result, the size of the main holes on the G-PVDF-2 membrane surface was remarkably reduced to 2 μm from the size of 5 μm of the pristine PVDF membrane (Fig. S5), as measured by the scale statistical software (Nano Measurer v1.2). The PVA coating of the holes on the G-PVDF-8 membrane surfaces prevented the hole measurement using this software (Fig. 1d). The bottom surfaces of these membranes were also observed. The observed morphological changes were similar to those of the top surface (Fig. S6), which indicated the same effect on both sides of the membrane surface induced by this method. The 3D AFM analyses also revealed that the

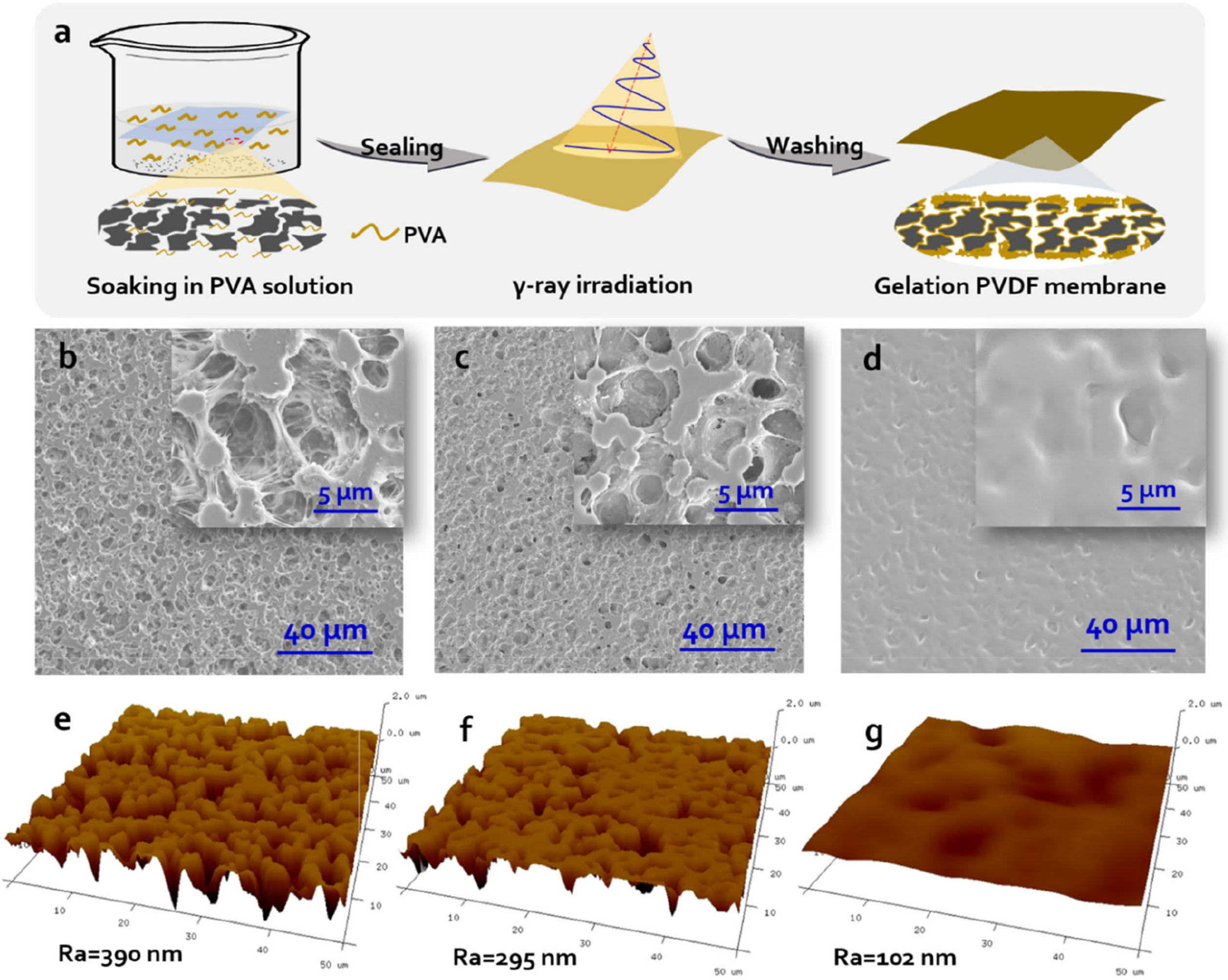

**Fig. 1** (Color online) **a** Schematic diagram of PVA in situ gelation in PVDF membranes under gamma irradiation; SEM images of **b** the pristine PVDF membrane, **c** G-PVDF-2 membrane, and **d** G-PVDF-8 membrane; 3-D AFM images of **e** the pristine PVDF membrane, **f** G-PVDF-2 membrane, and (g) G-PVDF-8 membrane

average roughness (Ra) values of the G-PVDF-2 and G-PVDF-8 membranes clearly declined to 295 and 102 nm, respectively, from the value of 390 nm of the pristine PVDF membranes (Figs. 1e–g). According to previous reports, the smooth surface built by PVA gelation could act as a protective layer and effectively lower the protein adsorption on the membrane surfaces [40].

SEM images of the membrane cross sections showed that the pristine PVDF membrane possessed a symmetrical structure and consisted of dense spongy pores (Figs. 2a–a″). After PVA modification, a distinct skin layer was observed on both surfaces of the G-PVDF membranes, with skin layer thicknesses of ~ 0.4 µm and 5 µm corresponding to the G-PVDF-2 and G-PVDF-8 membranes, respectively. This verified that the skin layer was directly related to the membrane DG (Figs. 2b–c″). In other words, the skin layer was easily tailored by controlling the soaking concentration of PVA. In addition, the rough and burr-like inner surface of the PVDF membrane pores (Fig. 2a″) was smoothened, and most of the internal pores with a small size in the membrane were filled in by the PVA gelation layer (Figs. 2b″, c″). To confirm this, the elemental composition of the membrane cross sections was measured using energy dispersive spectroscopy (EDS) mapping. As a result, O could be found throughout the membrane cross sections (Fig. S7). In addition, the O contents of the G-PVDF membranes were higher than those of the pristine PVDF and irradiated PVDF (i-PVDF, in water for 200 kGy of the total absorbed dose in 17 h) membranes, and increased with the soaking concentration of PVA (Fig. 3a). Additionally, the O distributions were more intense near the edge of the G-PVDF membrane cross section (Fig. S7), especially for the membranes with higher DGs. This was because a thicker PVA skin layer was constructed on the

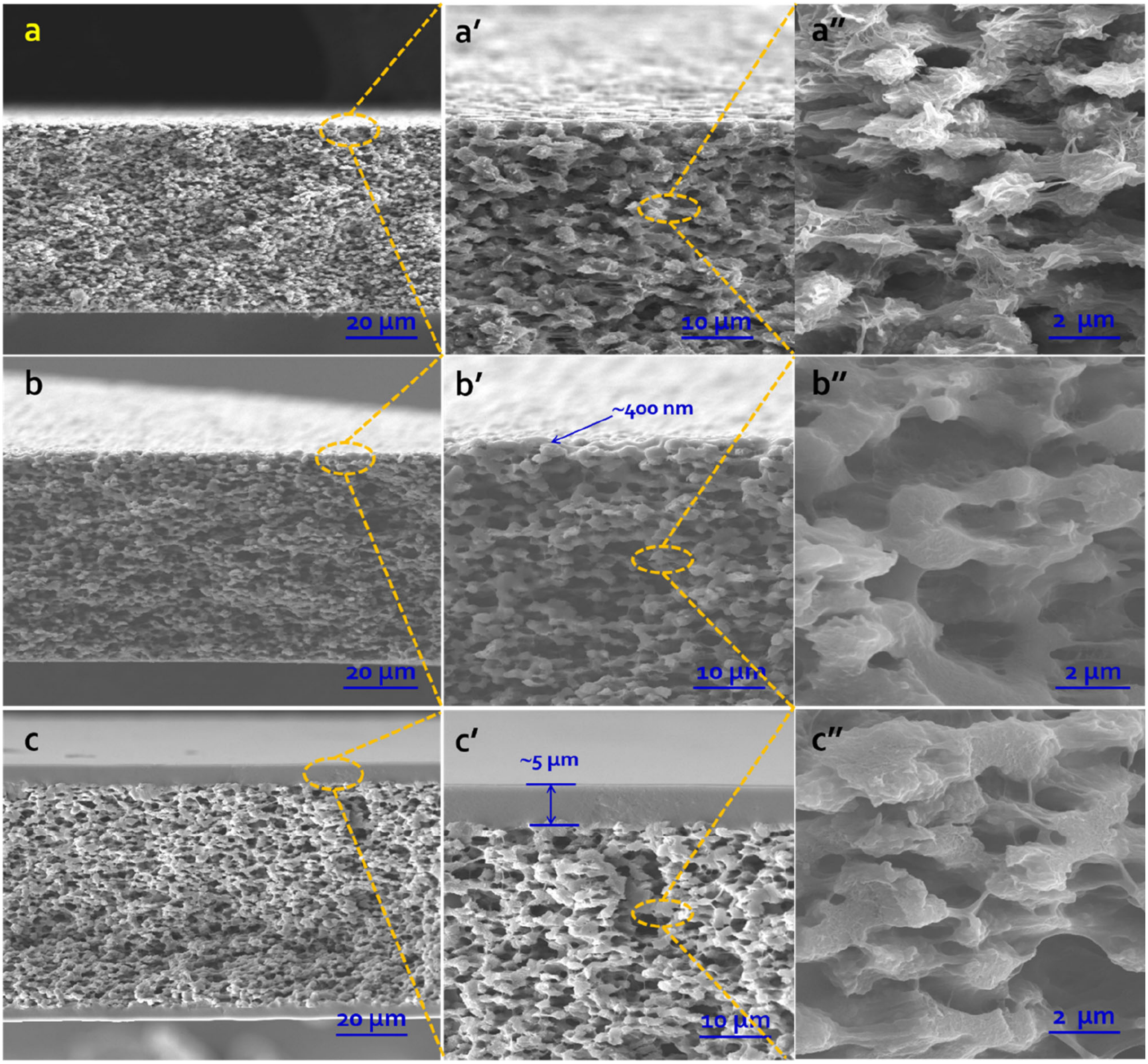

**Fig. 2** (Color online) SEM images of the cross section of the **a**, **a'**, **a''** pristine PVDF membrane, **b**, **b'**, **b''** G-PVDF-2 membrane, and **c**, **c'**, **c''** G-PVDF-8 membrane

membrane surface, which completely agreed with the observations in Figs. 2c–c″. Moreover, a significant increase in the O content of the G-PVDF membranes was observed in the central zone of the membrane cross section after PVA modification and was closely related to their DG (Figs. 3b and S8). Furthermore, the content of F decreased with the increase in the PVA DG, regardless of the entire or central zone of the membrane cross section (Table S1). These results confirmed that PVA was not only anchored on the membrane surfaces but also on the inner pore surfaces, thereby forming a hydrophilic layer on the membrane inside and outside, indicating the 3D modification of the PVDF membrane with the PVA layer under gamma-ray irradiation.

In order to verify that PVA was covalently attached to PVDF chains, we modified the PVDF powder with a PVA solution (2.5 wt%) under the same radiation conditions (see Experimental Sect. 2.1) and purified it using a large amount of hot water, which was confirmed by FT-IR spectroscopy (Fig. S9). Solid-state $^{13}$C-NMR spectroscopy (Figure S10) shows the peaks of $CH_2$ (∼ 47 ppm) and $CF_2$ (124.6 ppm) [41] and a new peak around 68.8 ppm appeared through deconvolution analysis, which could be attributed to the signal of CHOH, confirming the presence of PVA in the sample. Two peaks around 60 and 80.4 ppm

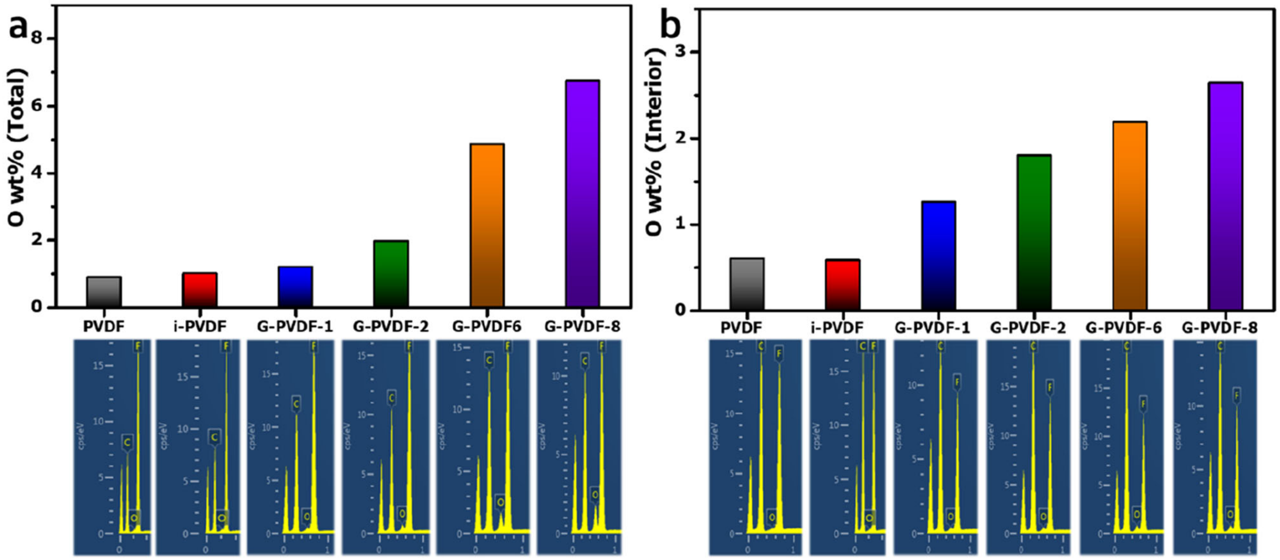

**Fig.3** (Color online) O content of different membranes measured by EDS mapping the **a** entire and **b** central zone of the membrane cross section. The insert images are the element compositions of different membranes from EDS mapping

were also observed, which could be attributed to the carbon atoms on the cross-linking points of the PVDF and PVA chains, respectively. The deshielding effect of electronegative groups decreased the electron density around the carbon atoms at the cross-linking points and subsequently resulted in their chemical shifts to lower field [42]. The solid-state $^{13}$C-NMR results provided powerful evidence for covalent bond formation between PVDF and PVA.

This mechanism can be explained by the principle of radiation chemistry. Water can be decomposed into hydrogen radicals (H$^{\cdot}$), hydroxyl radicals (HO$^{\cdot}$), and other active species by gamma-ray radiolysis [43]. The H$^{\cdot}$ and HO$^{\cdot}$ radicals can react with the PVA chains in an aqueous solution to generate polymeric radicals that combine with each other, resulting in PVA cross-linking [44]. In addition, these transient species from water radiolysis are able to initiate the formation of carbon-centered radicals on the PVDF chains [45]. Considering the high reactivity of radicals, it is reasonable to describe the formation of PVA gelation on the PVDF membrane surfaces and interiors in the following way: PVA radicals not only couple with other PVA radicals but also with PVDF radicals on the membrane surfaces and the pore inner surfaces when they are simultaneously irradiated with gamma-rays (Fig. S11). A similar phenomenon was observed and confirmed from the PVA modification of multiwalled carbon nanotubes via gamma-ray irradiation [46]. In contrast to conventional radiation-induced surface modification, this strategy is simple and convenient for modifying membranes with saturated macromolecules, rather than volatile, unstable, expensive, or unavailable vinyl monomers, which would be conducive to large-scale applications.

## 3.2 Fouling resistance of G-PVDF membranes

As mentioned above, both the membrane surfaces and the pore inner walls were covered by the PVA gelation layer, which altered the porous structure and inevitably affected water permeation through the resulting membranes. The water permeance through the G-PVDF membranes in a cross-flow filtration system (25 °C; 1 bar) was dramatically decreased in comparison with that through the pristine PVDF membranes and exhibited a negative correlation with the membrane DG (Fig. 4a). This was explained by the decreased porosity of these membranes, as PVA anchored on the membrane surface and the pore inner wall occupied a portion of the transport channels. However, the separation selectivity of the G-PVDF membranes was enhanced (Fig. 4b). The pristine PVDF membrane with a pore diameter of 450 nm was found to hardly reject PEG (or PEO) ranging from 11 to 600 kDa in molecular weight, but PEG (or PEO) rejection by the G-PVDF membranes improved as the DG was increased. By the well-documented definition, the MWCO and the mean pore diameter were calculated according to the curves of PEG (or PEO) rejection versus molecular weight (Fig. 4b and Table S2) [35]. The MWCOs of the G-PVDF-2, G-PVDF-6, and G-PVDF-8 membranes were 500, 173, and 16 kDa, and the corresponding mean pore diameters were 20.4, 6.8, and 4.6 nm, respectively. These results indicated that the pristine PVDF membrane converted from MF into UF by radiation-induced in situ PVA gelation across the membrane (the UF membrane criteria: the pore diameters range is 1–100 nm; MWCO ~ 500 kDa) [47]. In addition, the pore size distribution of the G-PVDF membranes,

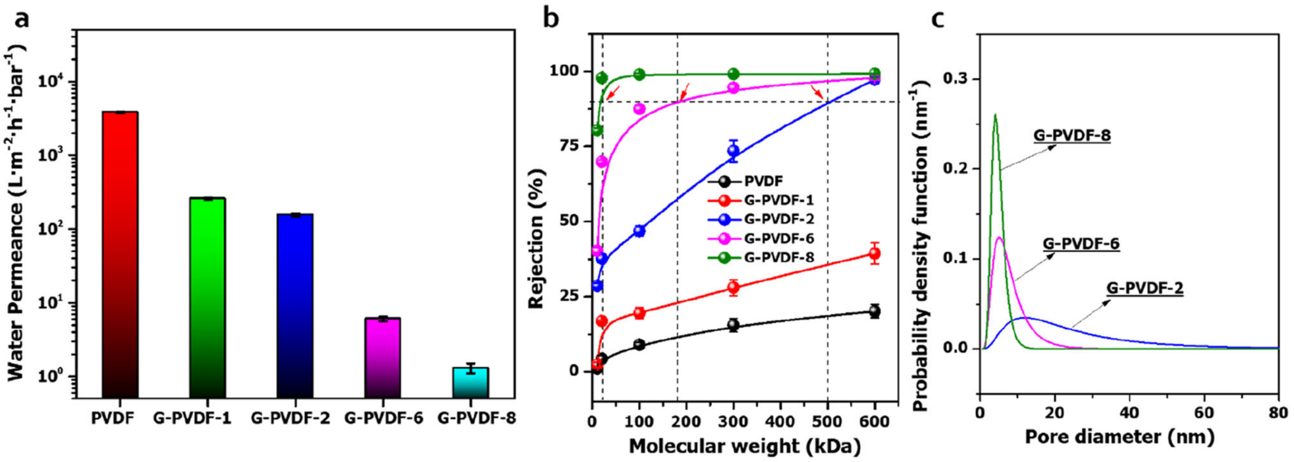

**Fig. 4** (Color online) **a** Water permeance of the pristine PVDF membrane and G-PVDF membrane; **b** plot of PEG rejection versus MWCO and **c** pore size distribution of the G-PVDF membranes

determined by PEG rejection experiments, was reduced and narrowed with increasing the membrane DG (Fig. 4c). This result indicated that the pore sizes of the G-PVDF UF membranes could be easily tuned by controlling the soaking concentration of PVA during membrane preparation.

Given that the membrane surfaces and the pore inner walls were finely covered by the PVA gelation layer, the water wettability on these surfaces was distinctly increased. The water contact angle (WCA) of these G-PVDF membranes monotonically decreased from 107° of the PVDF membranes to 37.6° of the G-PVDF-8 membranes, exhibiting an enhancement of the surface hydrophilicity, which was positively related to the membrane DG (Fig. 5a). The results of static fouling tests showed that the BSA adsorption capacity on the membranes was inversely proportional to the WCA of the membranes. This is because a lower WCA indicates higher surface hydrophilization and stronger repulsion of BSA from the membrane surface in a static fouling test (Fig. 5a) [48]. Despite similar WCAs, the BSA adsorption on the G-PVDF-1 membranes was still up to 26.8 $\mu g \cdot cm^{-2}$. However, on the G-PVDF-8 membranes, the BSA adsorption sharply reduced to 10.6 $\mu g \cdot cm^{-2}$ and then slowly to 6.4 $\mu g \cdot cm^{-2}$ when the DG was increased to 2.1%. This indicated that there was a DG threshold (2.1%) for the inhibition of protein adsorption on these membranes. This finding was interpreted to indicate the impact of DG on the amount of PVA coverage on the membrane surfaces and the pore inner walls as well as the pore size and distribution. These are important factors in BSA contact with membranes and diffusion into pores.

Although the fouling resistance was confirmed by WCA evaluations and static BSA adsorption measurements, the effects of PVA gelation on the membrane antifouling properties were further investigated through dynamic cross-flow fouling experiments (Fig. S12). These experiments are closer to the real process of membrane separation. Herein, the G-PVDF-2 membrane was used as a sample for its good permeation and selectivity (Fig. 4 and Table S2). As commonly used model globular proteins, BSA and lysozyme were selected as model membrane foulants. Three commonly used parameters: total fouling ($R_t$), reversible fouling ratio ($R_r$), and irreversible ratio ($R_{ir}$) were calculated using previously reported formulas to assess the membrane fouling resistance [36]. The flux recovery (FR) was determined from the pure water permeance ratio of the recycled to fresh membranes to evaluate the membrane recyclability. The pristine PVDF membrane was completely fouled by BSA ($R_t = 98\%$), and 95.3% of this fouling was irreversible (Fig. 5b). As a result, a very low water permeance was recovered to the recycled PVDF membrane ($FR = 6.6\%$), indicating severe BSA fouling, which rapidly deteriorated the membrane separation performance and shortened its lifetime. In contrast, the total fouling of the G-PVDF-2 membrane by BSA was only 54.2%, but 91.1% of this fouling was reversible, which represented a 95.1% water permeance recovery to the recycled G-PVDF-2 membrane. This demonstrated that the membrane after PVA modification exhibited excellent resistance to BSA fouling. This conclusion was also confirmed by lysozyme fouling experiments ($FR = 98.9\%$, $R_t = 17.9\%$, $R_r = 16.8\%$, and $R_{ir} = 1.1\%$) (Fig. 5c). In addition, the BSA and lysozyme rejection rates for the G-PVDF-2 membrane (9.35%, 43.54%) were higher than those of the pristine PVDF (2.67%, 12.37%) and i-PVDF (1.85%, 12.22%) membranes resulting from the blocking part of the membrane pores and the improvement of hydrophilicity by cross-linking the PVA layer (Fig. S13). It is worth noting that the resistance of the G-PVDF-2 membrane to lysozyme was significantly better than that of

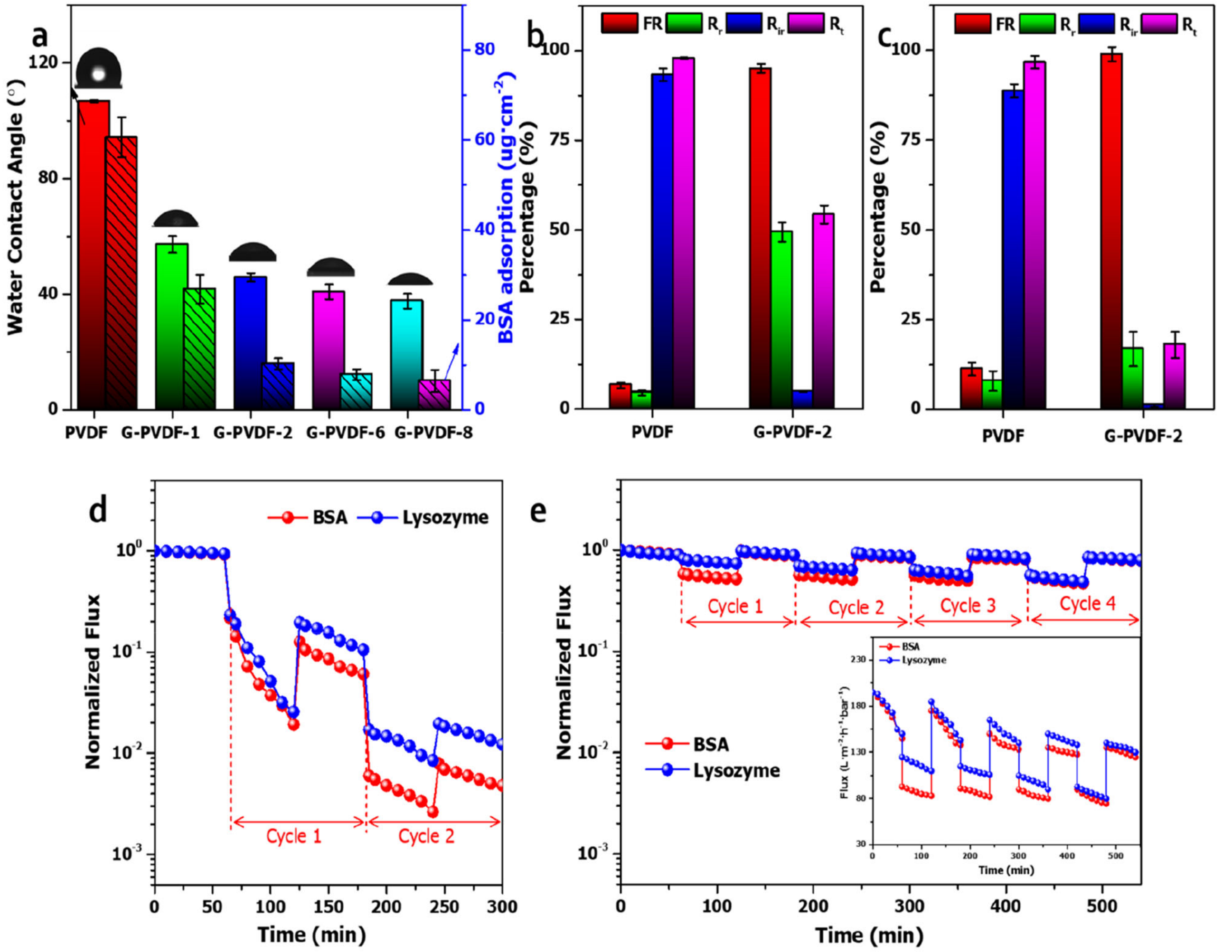

**Fig. 5** (Color online) **a** Water contact angle and static BSA adsorption of the membranes. The *FR*, $R_r$, $R_{ir}$ and $R_t$ values of the pristine PVDF membrane and G-PVDF-2 membrane fouled with **b** BSA and **c** lysozyme. The recyclability of (**d**) the pristine PVDF membrane and **e** G-PVDF-2 membrane after fouling in a BSA- or lysozyme-containing solution. The normalized flux was calculated as the ratio of the real-time flux to the initial water permeance ($J_t/J_0$). The testing was carried out in the following steps: water filtration, BSA or lysozyme solution (1 g·L$^{-1}$) filtration, and 15 min water backwashing. The cycle was repeated from water filtration

BSA. This result conflicted with the electrostatic principle because the PVDF membrane was electronegative owing to the high polarization of the C–F moieties [49], whereas BSA and lysozyme were negatively and positively charged, respectively, in the phosphate-buffered saline solution (pH 7.4) [50]. A reasonable explanation for this result is that the full PVA layer covered the membrane surfaces and the pore inner walls, resulting in a neutral G-PVDF-2 membrane and negligible Coulomb interactions. Instead, the hydrogen bonding ability of negatively charged BSA with PVA was higher than that of positively charged lysozyme. However, rod-like BSA (66.3 kDa, 14 nm × 3.8 nm × 3.8 nm) should easier stuck in the membrane pores than near-spherical lysozyme (14.4 kDa, 4.5 nm × 3 nm × 3 nm) [51], which reasonably explains the higher total fouling of the G-PVDF membranes from BSA than that from lysozyme (Figs. 5b–c).

To evaluate the membrane recyclability, fouling-backwashing cycle filtration tests were performed on a cross-flow device. When these membranes were used to treat a BSA or lysozyme solution, the filtration flux of the pristine PVDF membranes decreased by approximately two orders of magnitude in comparison with the pure water permeance of the fresh membranes (Fig. 5d). The pure water permeance returned to ~ 1% of the original value after two cycles, which indicated that the PVDF membranes had to be disposed in two cycles owing to severe and irreversible fouling in protein-containing solutions. The G-PVDF-2 membranes also experienced a flux decline when treated with a BSA or lysozyme solution, but their pure water permeance was almost completely recovered after backwashing with water for 15 min. Moreover, the FR of the G-PVDF-2 membranes maintained at more than 85% even after four cycles, whether fouled by BSA or lysozyme, indicating its long service life in membrane separation, cleanability, and recyclability (Fig. 5e). Thus, PVA gelation of the PVDF membranes was concluded to endow these membranes with hydrophilic and antifouling properties and to enhance their practicality in membrane separation because of their easy cleanability and good recyclability. In addition, the performances of the G-PVDF-2 membranes were compared with those of other modified PVDF membranes reported in recent years (Table S3). Although the pure water permeance was not the largest, the G-PVDF-2 membrane exhibited excellent water permeance recovery and ultralow irreversible fouling, and retained $> 85\%$ of the water permeance recovery after four cycles, indicating its outstanding antifouling and long-lasting properties.

### 3.3 Stability of the PVA layer to harsh chemical cleaning

As an integral part of a membrane system operation, chemical cleaning under acidic, alkaline, and/or oxidative conditions is required to remove stubborn foulants from membranes, regain their separation performance, and significantly impact the entire membrane process. Harsh chemical cleaning treatments are very likely to induce detachment of modifiers from the membrane and have adverse effects on the membrane integrity and service life [52]. Herein, the chemical stability of the G-PVDF-2 membranes, as a representative of G-PVDF membranes, was assessed by soaking in acidic (HCl, 1 $\mathrm{mol{\cdot}L^{-1}}$), alkaline (NaOH, 1 $\mathrm{mol{\cdot}L^{-1}}$), and oxidative (NaClO, 2 $\mathrm{g{\cdot}L^{-1}}$) solutions over time (24 h) at room temperature ($\sim$ 25 °C). Almost no weight loss was observed after soaking in the above-mentioned harsh solutions (Fig. 6a), but the WCAs on these membranes decreased after soaking treatment, especially on the membranes soaked in the NaOH solution (Fig. 6b). This result was attributed to the hydrolysis of acetate moieties from the PVA layer. A proof was provided by the FT-IR spectra of the G-PVDF-2 membranes before and after soaking in the harsh solutions. The spectra showed that the peak around 1720 $\mathrm{cm^{-1}}$ (acetate) disappeared in the three membranes after soaking in the HCl, NaOH, and NaClO solutions, separately (Fig. 6c). PVDF is widely reported to be vulnerable to alkaline environments, and both oxidative degradation and C=C bond formation can occur because of hydroxide ion attack [52]. Chemical changes on the PVDF membrane surfaces have also been confirmed by FT-IR spectra to occur during short- and long-term NaClO cleaning [52]. However, in our study, such changes, also assessed from FT-IR spectra, were not observed in pristine PVDF, even i-PVDF membranes, soaked in the aforementioned HCl, NaOH, and NaClO solutions for 24 h (Fig. S14). In comparison with a previous report [52], the poor hydrophilicity of the PVDF and i-PVDF membranes could account for the lack of signal changes detected from the FT-IR spectra of the membranes before and after soaking in the harsh solutions (Fig. S15). However, the hydrophilic G-PVDF-2 membrane after soaking in the harsh solutions still showed no changes in the FT-IR spectra, except for the disappearance of the acetate signal. The micromorphological examinations revealed that the surface of the G-PVDF-2 membranes was slightly roughened after soaking in the harsh solutions (Fig. S16). This could be explained by the acetate group hydrolysis of PVA, which caused the PVA layer to loosen and reassembly. Notwithstanding this, the main surface hole sizes maintained at $\sim$ 2 μm (Fig. S16), which demonstrated the chemical resistance of the G-PVDF-2 membrane to harsh chemical cleaning.

Although no signal changes were detected by FT-IR spectroscopy, the color of the pristine PVDF, i-PVDF, and G-PVDF-2 membranes obviously changed after soaking in the harsh solutions, especially in the NaOH solution (Fig. S17). To measure the color change quantitatively, the *Lab* values of the membranes were detected using a colorimeter. The *Lab* color model is a digital way to describe the visual perception of color, which is appropriate to define the color of materials quantitatively. In this model, the *L* value refers to the luminosity, and *a* value and *b* value denote the red/green and yellow/blue opponent colors, respectively [53]. The differences in the *L*, *a*, and *b* values of the membranes before and after soaking in the harsh solutions are shown in Fig. 7. It can be seen that the *L* value changes of the membranes soaked in the NaClO and HCl solutions were slight. However, when the membranes were soaked in the NaOH solution, the *L* values decreased, and the *a* and *b* values increased remarkably, which was consistent with the observations from digital pictures of the membranes (Fig. S17). The color changes of the i-PVDF membranes were significantly lower than those of the pristine PVDF membranes (Figs. 7a–b). This is because PVDF is generally prone to cross-linking under gamma-ray irradiation [29], whereas cross-linking turns its 2D linear structure into a 3D network, which significantly improves the mechanical properties and chemical resistance of PVDF membranes [54]. It should be noted that the G-PVDF-2 membranes showed the minimum color changes among the three tested membranes in the acidic, alkaline, or oxidative solution (Fig. 7c), indicating that the PVA gelation layer in the membrane enhanced the membrane tolerance to harsh chemical cleaning further.

Mechanical testing showed that the Young's modulus of the PVDF membranes was clearly improved after PVA

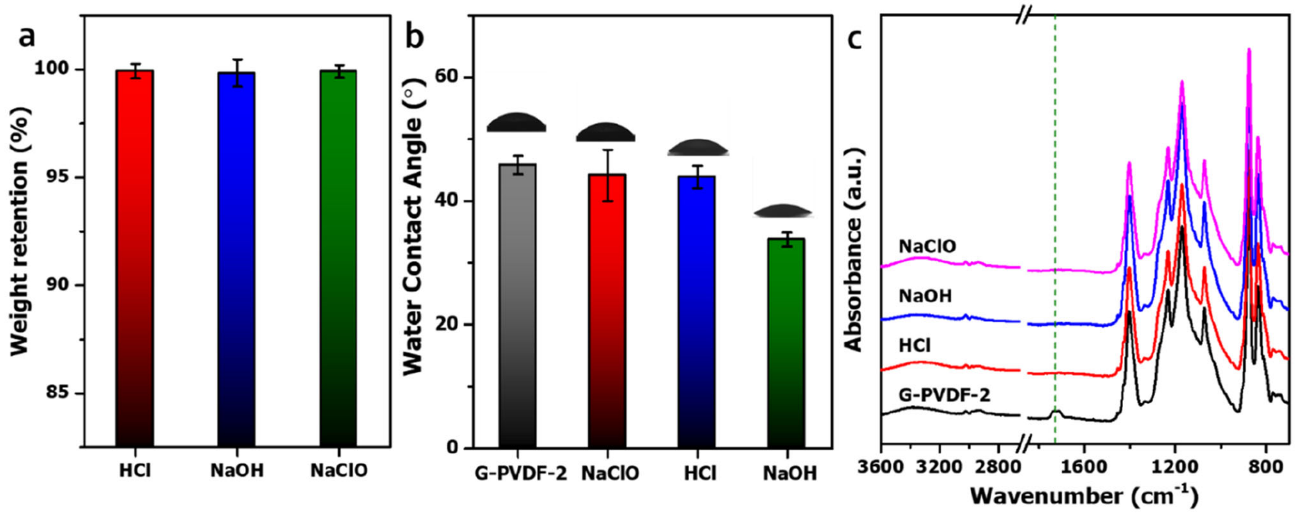

**Fig. 6** (Color online) **a** Weight retention, **b** water contact angle, and **c** FT-IR spectra of the G-PVDF-2 membrane before and after immersing in an HCl solution (1 mol· $L^{-1}$), a NaOH solution (1 mol· $L^{-1}$) and a NaClO solution (2 g·$L^{-1}$) for 24 h. The weight retention is the weight ratio of the membranes after immersion

in situ gelation in the membranes because of the radiation-induced (self-)cross-linking of PVDF and PVA, which indicated enhanced pressure-bearing performances of the PVDF membranes (Fig. 7d). The Young's moduli of the PVDF and i-PVDF membranes notably decreased after soaking under the harsh conditions, especially in the NaClO and NaOH solutions. In contrast, the G-PVDF-2 membranes showed relatively good resistance to chemical corrosion, even in the alkaline solutions, indicating that PVA gelation weakened corrosion by the HCl, NaOH, and NaClO aqueous solutions. Considering the PVA's good chemical stability of PVA, it was reasonable to infer that the PVA layer in the PVDF membrane acted as a physical barrier and protected bulk PVDF from chemical corrosion during the cleaning process. This suggests that full coverage with a chemically stable layer on membrane surfaces should be considered for extending membrane lifespans.

Additionally, the pure water permeance of the G-PVDF-2 membranes after harsh treatment exhibited a slight increase at the initial filtration stage, which might be due to the slightly increased pore size (Fig. 7e and Table S4). Of course, the PVA layer loosing and reassembly of the membranes caused by acetate group hydrolysis of PVA in the harsh solutions (Fig. S16) could also account for the mild change in the membrane filtration properties. Although the rejection ability of the membrane decreased slightly, the water permeance still recovered after two cycles of filtration and was on par with that of the fresh G-PVDF-2 membrane. This demonstrates that radiation-induced PVA in situ gelation through PVDF membranes improved the resistance of the membranes to chemical cleaning and maintained their antifouling performance.

### 3.4 Method universality investigation

It is well known that radiation-induced grafting has been widely used to prepare or modify various functional filtration membranes, which have even been industrialized in recent decades because of their universality. Comparatively speaking, the application of radiation-induced cross-linking to filtration membranes has not yet received sufficient attention. As mentioned above, the approach to permanent 3D modification of PVDF membranes is based on the intermolecular radical combination between PVA and PVDF and PVA itself. In other words, the cross-linking ability of modifiers and matrices is an essential requirement for successful membrane modification via radiation-induced cross-linking. To verify this viewpoint, other hydrophilic macromolecular modifiers, including PEG, SA, and PVP were used to modify the PVDF membrane through the same process as PVA under gamma-ray irradiation. Figure 8a shows a new absorption peak (~ 1660 $cm^{-1}$) in the FT-IR spectrum of the PVP-modified PVDF membrane, which is attributed to the characteristic peak of PVP. In contrast, the FT-IR spectrum of the membrane modified with PEG or SA showed no obvious absorption signals of the modifier (Figs. 8b–c). The DG measurements supported the observations of FT-IR spectroscopy. It was found that the DGs of the PVP-modified membrane were up to ~ 3%, similar to PVA, whereas both membranes modified with PEG and SA were almost unsuccessful in modifier anchoring (only ~ 0.1% of the DGs, Fig. S18). However, the WCA testing demonstrated that both the both modifications of the membranes with PEG and SA were successful because their WCAs were

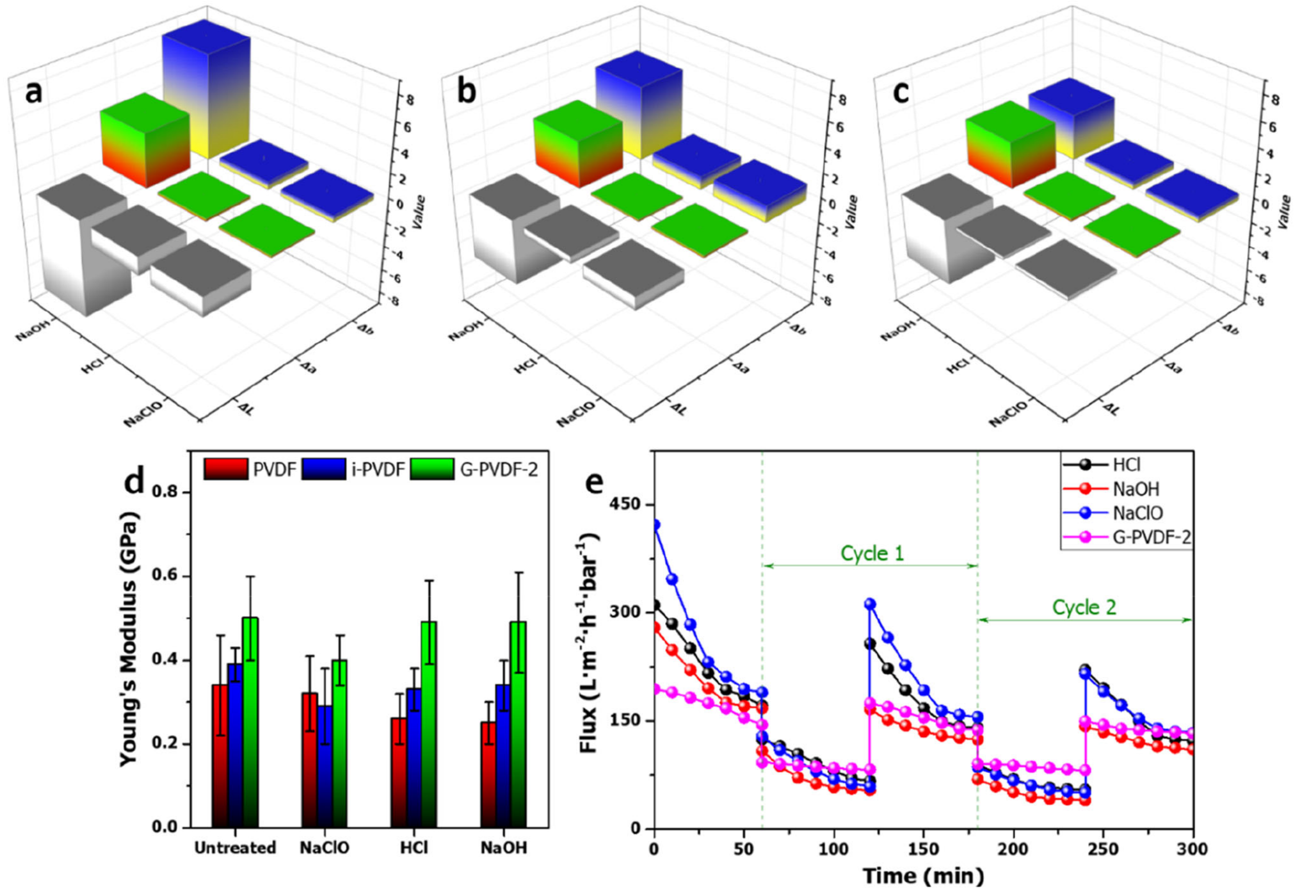

**Fig. 7** (Color online) Color changes of the **a** pristine PVDF membrane, **b** i-PVDF membrane, and **c** G-PVDF-2 membrane before and after soaking in harsh aqueous solutions (NaClO (2 g·L$^{-1}$), HCl (1 mol·L$^{-1}$), and NaOH (1 mol·L$^{-1}$)) for 24 h. All color changes were evaluated by differential *Lab* values. **d** Young's modulus of the pristine PVDF, i-PVDF, and G-PVDF-2 membranes before and after soaking in the above-mentioned harsh solutions, and **e** cycling filtration of a BSA-containing solution by using the G-PVDF-2 membranes before and after soaking in the harsh solutions above. The testing was carried out in the following steps: water filtration, BSA solution (1 g·L$^{-1}$) filtration, and 15 min water backwashing. The cycle was repeated from water filtration

notably lowered after gamma-ray treatment (~ 82.4° and ~ 68.6° corresponding to the membranes modified with PEG and SA, respectively). Moreover, their BSA adsorption in the static test also declined and showed a positive relationship with the WCA (Fig. 8d). The membrane modified with PVP showed the minimum WCA (~ 47.9°) and BSA adsorption (~ 11.6 μg cm$^{-2}$).

These results can be explained by different radiation chemistry effects of these three macromolecular modifiers under gamma-ray irradiation. In fact, PEG and SA are prone to degradation, and a few radiolysis fragments are probably anchored onto the PVDF skeleton by a random radical combination [55], resulting in lowered WCAs and BSA adsorption (Fig. 8d). However, these radiolysis fragments cannot be cross-linked to form a gelation layer on or in the membranes as PVA (Figs. S19a–a', S19b–b'), corresponding to their extremely low DGs. In comparison, PVP is inclined to form a hydrogel via radiation-induced self-cross-linking. Thus, PVP not only was anchored onto the PVDF skeleton but also formed a gelation layer on or in the PVDF membrane (Figs. S19c–c'), leading to the highest hydrophilicity and the lowest BSA adsorption (Fig. 8d). Given the above, it is clear that directly treating macromolecular modifiers and membrane matrices under gamma-ray irradiation is universal to endow membrane materials with good hydrophilicity and excellent antifouling performance, especially using modifiers with a higher trend for radiation-induced cross-linking than that for degradation.

## 4 Conclusion

In summary, a permanent 3D modification method for antifouling PVDF membrane preparation was developed through radiation-induced cross-linking between the membrane matrix and hydrophilic macromolecular modifiers. Thus, the membrane surfaces and the pore inner

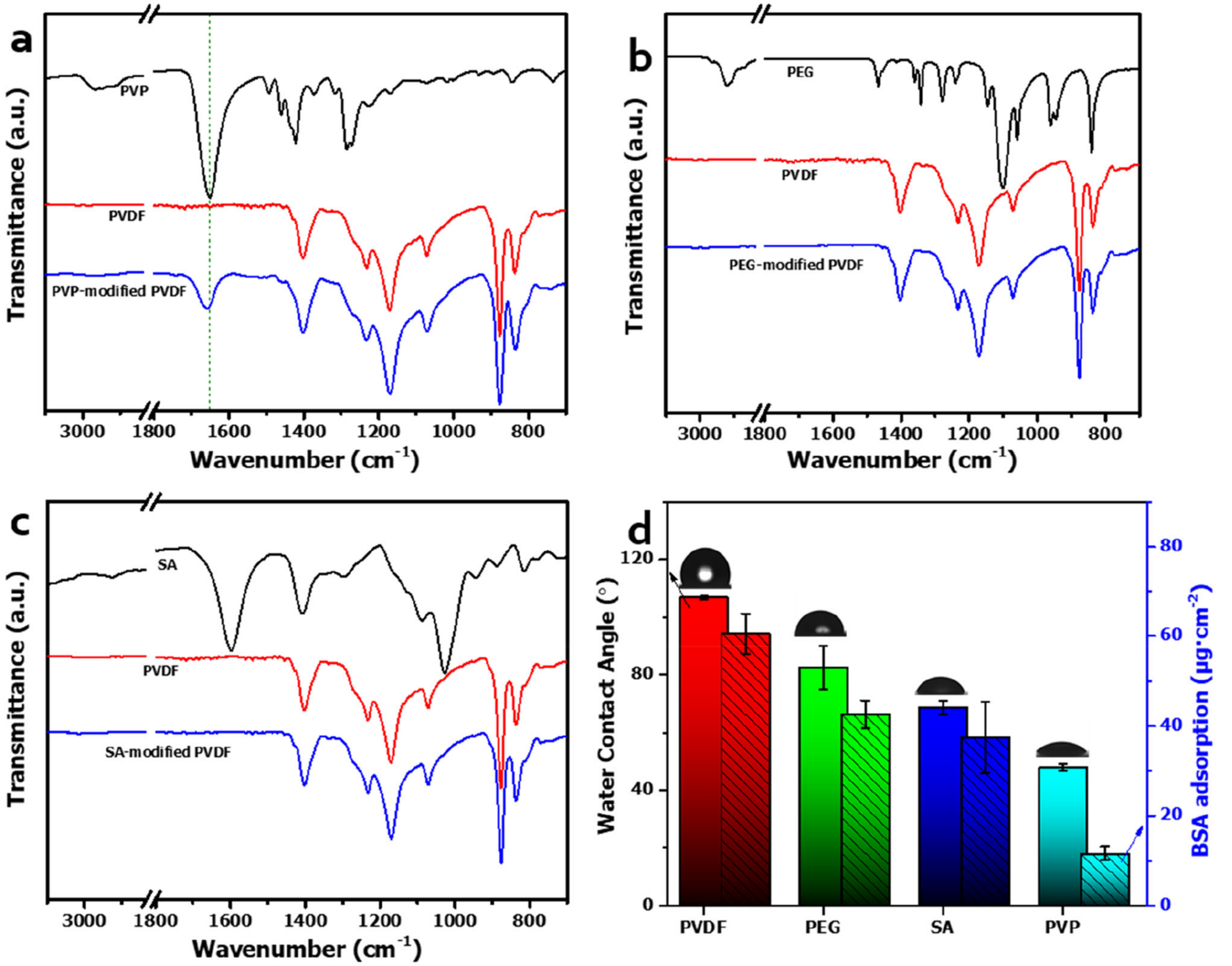

**Fig. 8** (Color online) FT-IR spectra of the modified PVDF membranes by different modifiers: **a** PVP, **b** PEG, and **c** SA; **d** water contact angle of and static BSA adsorption of the PVDF membranes modified by different modifiers

surfaces were effectively modified with PVA gelation layers, which smoothened the membrane surfaces and enhanced their hydrophilicity and resistance to protein adsorption. In addition, the pore size and distribution of the membranes could be effectively tuned by controlling the PVA concentration to meet the needs of different rejection requirements in filtration, even converting a hydrophobic MF membrane to a hydrophilic UF form. The resultant G-PVDF membranes showed very low total and irreversible fouling rates ($< 5\%$) in protein solutions and a high flux recovery ($> 95\%$) with water rinsing. In addition, multicycle filtration tests confirmed that these G-PVDF membranes were recycled well with water rinsing, which indicated their good cleanability, recyclability, and potential benefits in their applications for separation processes. Meanwhile, owing to the stable PVA gelation layer, the G-PVDF membranes exhibited good resistance to chemical cleaning in an acidic, alkaline, or NaClO solution and maintained good antifouling performance. Furthermore, the universality of this 3D modification method was investigated by replacing PVA with other water-soluble polymers (such as PEG, SA, and PVP) as modifiers. The results clearly confirmed the improved hydrophilicity and resistance to protein fouling of the modified PVDF membranes. Overall, the new concepts of this 3D modification via radiation-induced cross-linking would open up an interesting research strategy for developing functional membrane materials for a variety of applications.

**Acknowledgements** The authors would like to thank Prof. Wan-Zhong Lang and his group from Shanghai Normal University for their enthusiastic help and support for the characterization of membranes, and they also have pleasure in acknowledging the support from the Shanghai Engineering Research Centre of Green Energy Chemical Engineering.

**Author contributions** All authors contributed to the study conception and design. Material preparation, data collection and analysis were performed by Yu Gu and Bo-Wu Zhang. The first draft of the manuscript was written by Yu Gu and all authors commented on previous versions of the manuscript. All authors read and approved the final manuscript.

## References

1. X. Zhao, R. Zhang, Y. Liu et al., Antifouling membrane surface construction: chemistry plays a critical role. J. Membrane Sci. **551**, 145–171 (2018). https://doi.org/10.1016/j.memsci.2018.01.039
2. V. Kochkodan, D.J. Johnson, N. Hilal, Polymeric membranes: Surface modification for minimizing (bio)colloidal fouling. Adv. Colloid Interface Sci. **206**, 116–140 (2014). https://doi.org/10.1016/j.cis.2013.05.005
3. S.A. Deowan, F. Galiano, J. Hoinkis et al., Novel low-fouling membrane bioreactor (MBR) for industrial wastewater treatment. J. Membrane Sci. **510**, 524–532 (2016). https://doi.org/10.1016/j.memsci.2016.03.002
4. S.H. Woo, J. Park, B.R. Min, Relationship between permeate flux and surface roughness of membranes with similar water contact angle values. Sep. Purif. Technol. **146**, 187–191 (2015). https://doi.org/10.1016/j.seppur.2015.03.048
5. Z. Jiang, S. Karan, A.G. Livingston, Membrane fouling: does microscale roughness matter? Ind. Eng. Chem. Res. **59**, 5424–5431 (2020). https://doi.org/10.1021/acs.iecr.9b04798
6. Y. Hu, Z. Lü, C. Wei et al., Separation and antifouling properties of hydrolyzed PAN hybrid membranes prepared via in-situ sol–gel $SiO_2$ nanoparticles growth. J. Membrane Sci. **545**, 250–258 (2018). https://doi.org/10.1016/j.memsci.2017.09.081
7. X. Tan, C. Hu, Z. Zhu et al., Electrically pore-size-tunable polypyrrole membrane for antifouling and selective separation. Adv. Funct. Mater. **29**, 1903081 (2019). https://doi.org/10.1002/adfm.201903081
8. S. Ghiasi, A. Behboudi, T. Mohammadi et al., Effect of surface charge and roughness on ultrafiltration membranes performance and polyelectrolyte nanofiltration layer assembly. Colloids Surf. A **580**, 123753 (2019). https://doi.org/10.1016/j.colsurfa.2019.123753
9. H. Jiang, Q. Zhao, P. Wang et al., Improved separation and antifouling properties of PVDF gravity-driven membranes by blending with amphiphilic multi-arms polymer PPG-Si-PEG. J. Membrane Sci. **588**, 117148 (2019). https://doi.org/10.1016/j.memsci.2019.05.072
10. K.M. Dobosz, C.A. Kuo-LeBlanc, T. Emrick et al., Antifouling ultrafiltration membranes with retained pore size by controlled deposition of zwitterionic polymers and poly(ethylene glycol). Langmuir **35**, 1872–1881 (2019). https://doi.org/10.1021/acs.langmuir.8b02184
11. J.H. Zuo, Y.H. Gu, C. Wei et al., Janus polyvinylidene fluoride membranes fabricated with thermally induced phase separation and spray-coating technique for the separations of both W/O and O/W emulsions. J. Membrane Sci. **595**, 117475 (2020). https://doi.org/10.1016/j.memsci.2019.117475
12. Y. Zhao, X. Yang, L. Yan et al., Biomimetic nanoparticle-engineered superwettable membranes for efficient oil/water separation. J. Membrane Sci. **618**, 118525 (2021). https://doi.org/10.1016/j.memsci.2020.118525
13. Z. Lin, C. Hu, X. Wu et al., Towards improved antifouling ability and separation performance of polyethersulfone ultrafiltration membranes through poly(ethylenimine) grafting. J. Membrane Sci. **554**, 125–133 (2018). https://doi.org/10.1016/j.memsci.2018.02.065
14. Z.-Y. Liu, Q. Jiang, Z. Jin et al., Understanding the antifouling mechanism of zwitterionic monomer-grafted polyvinylidene difluoride membranes: a comparative experimental and molecular dynamics simulation study. ACS Appl. Mater. Interfaces **11**, 14408–14417 (2019). https://doi.org/10.1021/acsami.8b22059
15. L. Han, Y.Z. Tan, C. Xu et al., Zwitterionic grafting of sulfobetaine methacrylate (SBMA) on hydrophobic PVDF membranes for enhanced anti-fouling and anti-wetting in the membrane distillation of oil emulsions. J. Membrane Sci. **588**, 117196 (2019). https://doi.org/10.1016/j.memsci.2019.117196
16. R. Zhang, Y. Liu, M. He et al., Antifouling membranes for sustainable water purification: strategies and mechanisms. Chem. Soc. Rev. **45**, 5888–5924 (2016). https://doi.org/10.1039/C5CS00579E
17. T.A. Trinh, W. Li, J.W. Chew, Internal fouling during microfiltration with foulants of different surface charges. J. Membrane Sci. **602**, 117983 (2020). https://doi.org/10.1016/j.memsci.2020.117983
18. H. Sun, X. Yang, Y. Zhang et al., Segregation-induced in situ hydrophilic modification of poly(vinylidene fluoride) ultrafiltration membranes via sticky poly(ethylene glycol) blending. J. Membrane Sci. **563**, 22–30 (2018). https://doi.org/10.1016/j.memsci.2018.05.046
19. J. Zhao, X. Zhao, Z. Jiang et al., Biomimetic and bioinspired membranes: Preparation and application. Prog. Polym. Sci. **39**, 1668–1720 (2014). https://doi.org/10.1016/j.progpolymsci.2014.06.001
20. B. Wu, B. Zhang, J. Wu et al., Electrical switchability and dry-wash durability of conductive textiles. Sci. Rep. **5**, 11255 (2015). https://doi.org/10.1038/srep11255
21. R.L. Clough, High-energy radiation and polymers: a review of commercial processes and emerging applications. Nucl. Instrum. Methods Phys. Res. Sect. B Beam Interact. Mater. Atoms **185**, 8–33 (2001). https://doi.org/10.1016/S0168-583X(01)00966-1
22. S.-T. Ji, Q.-Q. Wang, J. Zhou et al., Synthesis of a Ag/AgCl/PLA membrane under electron beam irradiation for the photocatalytic degradation of methylene blue and chloramphenicol. Nucl. Sci. Tech. **31**, 22 (2020). https://doi.org/10.1007/s41365-020-0726-8
23. X. Xu, X.-J. Ding, J.-X. Ao et al., Preparation of amidoxime-based PE/PP fibers for extraction of uranium from aqueous solution. Nucl. Sci. Tech. **30**, 20 (2019). https://doi.org/10.1007/s41365-019-0543-0
24. M.M. Nasef, O. Güven, Radiation-grafted copolymers for separation and purification purposes: Status, challenges and future directions. Prog. Polym. Sci. **37**, 1597–1656 (2012). https://doi.org/10.1016/j.progpolymsci.2012.07.004
25. J. Ye, B. Zhang, Y. Gu et al., Tailored graphene oxide membranes for the separation of ions and molecules. ACS Appl. Nano Mater. **2**, 6611–6621 (2019). https://doi.org/10.1021/acsanm.9b01356
26. M.M. Nasef, E.-S.A. Hegazy, Preparation and applications of ion exchange membranes by radiation-induced graft copolymerization of polar monomers onto non-polar films. Prog. Polym. Sci. **29**, 499–561 (2004). https://doi.org/10.1016/j.progpolymsci.2004.01.003
27. M.M. Nasef, S.A. Gürsel, D. Karabelli et al., Radiation-grafted materials for energy conversion and energy storage applications. Prog. Polym. Sci. **63**, 1–41 (2016). https://doi.org/10.1016/j.progpolymsci.2016.05.002
28. J.H. O'Donnell, Radiation Chemistry of Polymers, in *The effects of radiation on high-technology polymers. ACS Symposium Series*, vol. 381, (American Chemical Society, 1989), pp. 1–13

29. J.S. Forsythe, D.J.T. Hill, The radiation chemistry of fluoropolymers. Prog. Polymer Sci. **25**, 101–136 (2000). https://doi.org/10.1016/S0079-6700(00)00008-3
30. Y. Iwai, A. Hiroki, M. Tamada, Radiation-induced crosslinking of Nafion® N117CS membranes. J. Membrane Sci. **369**, 397–403 (2011). https://doi.org/10.1016/j.memsci.2010.12.027
31. D. Rana, B.M. Mandal, S.N. Bhattacharyya, Miscibility and phase diagrams of poly(phenyl acrylate) and poly(styrene-co-acrylonitrile) blends. Polymer **34**, 1454–1459 (1993). https://doi.org/10.1016/0032-3861(93)90861-4
32. D. Rana, K. Bag, S.N. Bhattacharyya et al., Miscibility of poly(styrene-co-butyl acrylate) with poly(ethyl methacrylate): existence of both UCST and LCST. J. Polym. Sci. Poly. Phys. **38**, 369–375 (2000). https://doi.org/10.1002/(SICI)1099-0488(20000201)38:3%3c369::AID-POLB3%3e3.0.CO;2-W
33. J. Zhang, Z. Wang, Q. Wang et al., Relationship between polymers compatibility and casting solution stability in fabricating PVDF/PVA membranes. J. Membrane Sci. **537**, 263–271 (2017). https://doi.org/10.1016/j.memsci.2017.05.041
34. K. Zhu, Y. Mu, M. Zhang et al., Mixed matrix membranes decorated with in situ self-assembled polymeric nanoparticles driven by electrostatic interaction. J. Mater. Chem. A **6**, 7859–7870 (2018). https://doi.org/10.1039/C8TA00317C
35. P.H.H. Duong, S. Chisca, P.Y. Hong et al., Hydroxyl functionalized polytriazole-*co*-polyoxadiazole as substrates for forward osmosis membranes. ACS Appl. Mater. Interfaces **7**, 3960–3973 (2015). https://doi.org/10.1021/am508387d
36. Y. Li, S. Huang, S. Zhou et al., Enhancing water permeability and fouling resistance of polyvinylidene fluoride membranes with carboxylated nanodiamonds. J. Membrane Sci. **556**, 154–163 (2018). https://doi.org/10.1016/j.memsci.2018.04.004
37. B. Wang, M. Kodama, S. Mukataka et al., On the intermolecular crosslinking of PVA chains in an aqueous solution by γ-ray irradiation. Polym. Gels Netw. **6**, 71–81 (1998). https://doi.org/10.1016/S0966-7822(98)00003-3
38. G. Beamson, D. Briggs, *High Resolution XPS of Organic Polymers: The Scienta ESCA300 Database* (Wiley, Chichester, 1992)
39. A. Qin, X. Li, X. Zhao et al., Engineering a highly hydrophilic PVDF membrane via binding tio2 nanoparticles and a PVA layer onto a membrane surface. ACS Appl. Mater. Interfaces **7**, 8427–8436 (2015). https://doi.org/10.1021/acsami.5b00978
40. J.R. Du, S. Peldszus, P.M. Huck et al., Modification of poly(vinylidene fluoride) ultrafiltration membranes with poly(-vinyl alcohol) for fouling control in drinking water treatment. Water Res. **43**, 4559–4568 (2009). https://doi.org/10.1016/j.watres.2009.08.008
41. T. Montina, P. Wormald, P. Hazendonk, 13C solid-state NMR of the mobile phase of poly(vinylidene fluoride). Macromolecules **45**, 6002–6007 (2012). https://doi.org/10.1021/ma3013477
42. H. Jang, D.H. Song, I.C. Kim et al., Fouling control through the hydrophilic surface modification of poly(vinylidene fluoride) membranes. J. Appl. Polym. Sci. **132**, 41712 (2015). https://doi.org/10.1002/app.41712
43. J.M. Rosiak, Hydrogel dressings, in *Radiation Effects on Polymers. ACS Symposium Series*, vol. 475, (American Chemical Society, 1991), pp. 271–299
44. W. Chen, H. Bao, M. Zhang, Effect of gamma radiation on gelation in polyvinyl alcohol solutions. Radiat. Phys. Chem. **26**, 43–47 (1985). https://doi.org/10.1016/0146-5724(85)90031-7
45. T.R. Dargaville, G.A. George, D.J.T. Hill et al., High energy radiation grafting of fluoropolymers. Prog. Polym. Sci. **28**, 1355–1376 (2003). https://doi.org/10.1016/S0079-6700(03)00047-9
46. Y. Gu, H. Li, L. Liu et al., Constructing CNTs-based composite membranes for oil/water emulsion separation via radiation-induced “grafting to” strategy. Carbon **178**, 678–687 (2021). https://doi.org/10.1016/j.carbon.2021.03.051
47. A. Lee, J.W. Elam, S.B. Darling, Membrane materials for water purification: design, development, and application. Environ. Sci. Water Res. Technol. **2**, 17–42 (2016). https://doi.org/10.1039/C5EW00159E
48. Y. Zhao, J. Wen, H. Sun et al., Thermo-responsive separation membrane with smart anti-fouling and self-cleaning properties. Chem. Eng. Res. Des. **156**, 333–342 (2020). https://doi.org/10.1016/j.cherd.2020.02.006
49. Y. Zhang, J. Wang, F. Gao et al., A comparison study: the different impacts of sodium hypochlorite on PVDF and PSF ultrafiltration (UF) membranes. Water Res. **109**, 227–236 (2017). https://doi.org/10.1016/j.watres.2016.11.022
50. X. Yang, B. Zhang, Z. Liu et al., Preparation of the antifouling microfiltration membranes from poly(*N*,*N*-dimethylacrylamide) grafted poly(vinylidene fluoride) (PVDF) powder. J. Mater. Chem. **21**, 11908–11915 (2011). https://doi.org/10.1039/C1JM11348H
51. S. Bhattacharjee, R. Kumar, K.S. Gandhi, Modelling of protein mixture separation in a batch foam column. Chem. Eng. Sci. **56**, 5499–5510 (2001). https://doi.org/10.1016/S0009-2509(01)00156-7
52. M.F. Rabuni, N.M. Nik Sulaiman, N. Awanis Hashim, A systematic assessment method for the investigation of the PVDF membrane stability. Desalin. Water Treat. **57**, 1–12 (2016). https://doi.org/10.1080/19443994.2015.1012336
53. X. Ding, M. Yu, Z. Wang et al., A promising clean way to textile colouration: cotton fabric covalently-bonded with carbon black, cobalt blue, cobalt green, and iron oxide red nanoparticles. Green Chem. **21**, 6611–6621 (2019). https://doi.org/10.1039/C9GC02084E
54. C. Yang, G. Wu, Chapter Four—Radiation Cross-Linking for Conventional and Supercritical $CO_2$ Foaming of Polymer, in *Radiation Technology for Advanced Materials*. ed. by G. Wu, M. Zhai, M. Wang (Academic Press, 2019), pp. 115–139
55. Y. Gu, Y. Qiao, Y. Meng et al., One-step synthesis of well-dispersed polypyrrole copolymers under gamma-ray irradiation. Polym. Chem. **12**, 645–649 (2021). https://doi.org/10.1039/D0PY01566K